Chapter 9

Electroweak Physics

9.1 Production of W and Z bosons

9.1.1 Introduction

The reactions $pp \to W + X$ and $pp \to Z + X$ with subsequent leptonic decays of the massive electroweak vector bosons, $W \to \ell\nu$ and $Z \to \ell^+\ell^-$, have a large cross section and are theoretically well understood. Cross sections above 10 nb (1 nb) are expected at the LHC for the $W \to \ell\nu$ ($Z \to \ell^+\ell^-$) channel in the fiducial region of the CMS detector. Hence these reactions are useful for many purposes, including a precise luminosity monitor, a high-statistics detector calibration tool and to demonstrate the performance of the CMS experiment. These reactions will be among the first to be measured at the LHC.

Here we discuss prospects for precise measurements of the reactions $pp \to Z + X$ and $pp \to W + X$ at the LHC using the decays of the gauge bosons into electrons and muons. Studies have been performed based on Monte Carlo samples generated with PYTHIA including realistic detector simulation and addressing the most relevant systematic effects. The potentially most dangerous background in these analyses consists of QCD events with leptons from hadron decays or tracks misidentified as leptons. However, these lepton candidates are associated to jets and can be largely suppressed using isolation algorithms.

Robust criteria are developed which allow for a low-background event selection which is rather insensitive to detector inhomogeneities. This robust selection is considered as especially useful for the CMS startup phase. The results show that a determination of the W and Z rates with an experimental precision on the percent level is feasible already in the early phase of the experiment.

9.1.2 W/Z into electrons

The process $\mathrm{pp} \to \mathrm{ZX}$ and $\mathrm{pp} \to \mathrm{WX}$ with subsequent decay of Z and W into electrons is studied using the full CMS detector simulation and analysis scheme. The aim is to define some baseline selection which is suppressing background to a very small level and detector inhomogeneities can be controlled. This selection can thus be considered as especially useful for the CMS startup phase. Details can be found in [340].

Electron (positron) candidates are selected with the following criteria [312]:

- The minimal E_{T} of the electromagnetic cluster has to be larger than 20 GeV with $|\eta_{\mathrm{cluster}}| < 1.4$ for barrel electron candidates and $1.6 < |\eta_{\mathrm{cluster}}| < 2.4$ for endcap electron candidates.
- The cluster should be consistent with the shower shape expected for electromag-

netic showers. The spread of the electromagnetic shower along the η direction is rather insensitive to bremsstrahlung, thus allowing a good separation of signal and background shower shapes. Therefore it is required that the spread of the electromagnetic shower in η with respect to η of the supercluster, $\sigma_{\eta\eta}$, is smaller than 0.01.

- The energy deposit in the associated hadron calorimeter cluster should be very small. For this selection the ratio $E_{\mathrm{Had}}/E_{\mathrm{EM}}$ has to be smaller than 0.05.
- In order to be identified as an electron, a reconstructed track has to be matched with the cluster such that $\Delta R < 0.15$ (where $\Delta R = \sqrt{\Delta\phi^2 + \Delta\eta^2}$). Furthermore, it is required that the ratio of the cluster energy and the track momentum, E/P, is larger than 0.9 and that $|1/E - 1/P| < 0.02$.
- Finally, it is required that the electron candidate is isolated. The transverse momentum sum of all other tracks found within a cone radius ΔR of 0.35 divided by the electron candidate transverse supercluster energy has to be smaller than 0.2. Only tracks with a transverse momentum above 1.5 GeV/c and with at least four hits in the central tracker which are close to the interaction vertex are considered.

9.1.2.1 $pp \to Z \to eeX$ Selection

We analyse events where one $\mathrm{e^+e^-}$ pair consistent with the Z mass is found (if more than two electrons pass the selection criteria, only those two with the highest transverse momenta are considered). The generated and reconstructed mass distribution are shown in Figure 9.1 left. For now, the "electron" clusters are not corrected for bremsstrahlung within the tracker and the reconstructed Z peak is found to be about 1 GeV lower than the generated one.

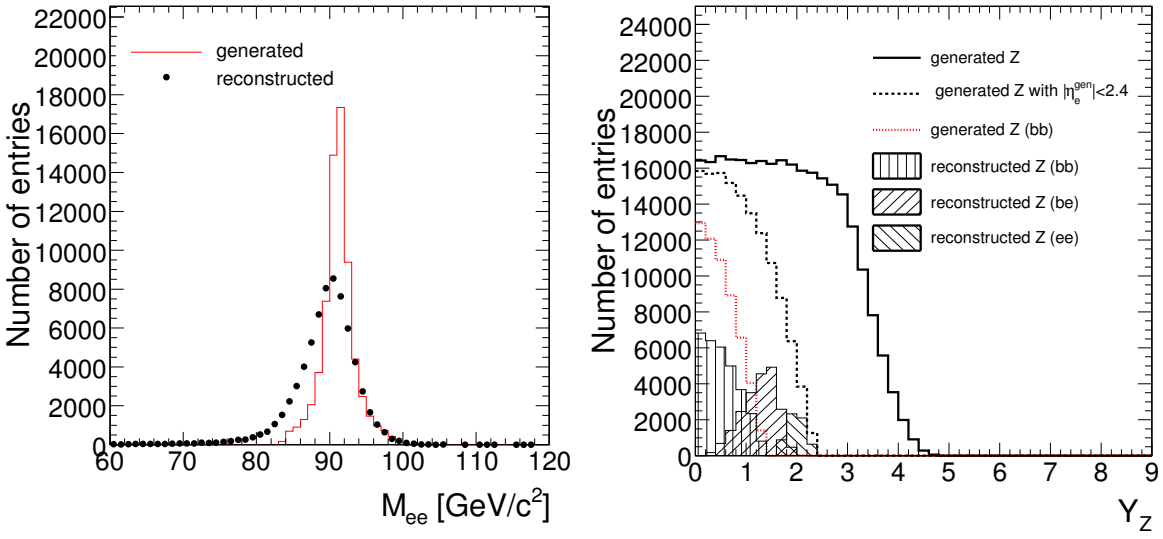

Figure 9.1: Left: Reconstructed and generated Z mass distribution with all cuts. Right: Generated rapidity distribution for all Z candidates and for those where both electrons were generated within the geometrical acceptance of the electromagnetic calorimeter. For comparison, the rapidity distribution of the finally accepted Z events is already shown here.

Using this selection, the rapidity distribution of the accepted Z events is shown in Figure 9.1 right. In addition, the rapidity distribution of the potentially accepted Z bosons, separated

for the three cases where both decay electrons are within the acceptance of the barrel calorimeter (BB) $|\eta_{\mathrm{BB}}| < 1.4$, both within the endcaps (EE) $1.6 < |\eta_{\mathrm{EE}}| < 2.4$ or one within the barrel and the other one in the endcaps (EB) are also shown. In the case that both generated electrons are in the barrel, a Z detection efficiency of about 60% is reached.

Here the electron efficiency is defined by the ratio of reconstructed electrons from accepted Z events to the number of electrons from generated Z events, where the generated electrons fulfilled the condition $|\eta^{\mathrm{e}}_{\mathrm{gen}}| < 1.4$. Figure 9.2 left shows the efficiency distribution for all supermodules folded such that the local ϕ angle for all odd supermodules goes from 0-20 degrees and for all even supermodules from 20-40 degrees.

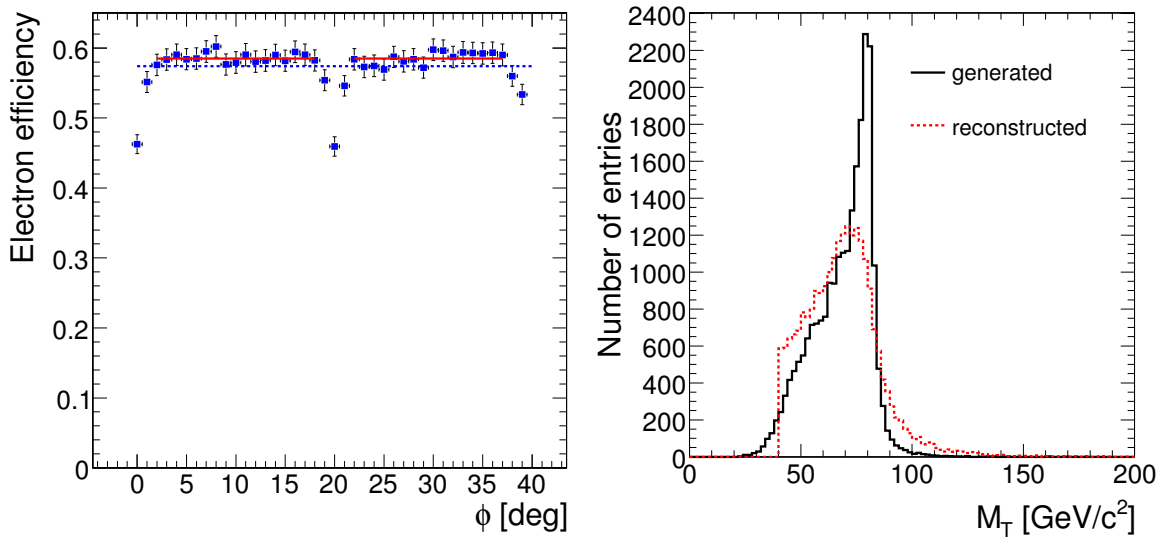

Figure 9.2: Left: The electron reconstruction efficiency in $\mathrm{Z} \rightarrow \mathrm{e^+e^-}$ events as a function of ϕ, all even and odd numbered supermodules are folded such that the odd (even) numbered supermodules always cover local ϕ angles from 0 to 20 degrees and from 20 to 40 degrees respectively. The dotted line corresponds to the average efficiency $57.3 \pm 0.2\%$ over the whole ϕ range and the solid lines correspond to the average efficiency $58.4 \pm 0.2\%$ with the gap regions excluded. Right: Generated (solid line) and reconstructed (dashed line) transverse W mass. The W transverse mass is reconstructed from the electron four-momentum and the missing transverse energy. In this plot, only events with no reconstructed jet above 20 GeV transverse energy are included.

The efficiency drop of about 10% between the supermodules is clearly visible with the available sample of Z events corresponding to roughly $0.2\,\mathrm{fb}^{-1}$. Similar inefficiencies were found in the η direction at supermodule boundaries. From the analysis of the reconstruction efficiency as function of the phi angle, we get an efficiency of $27.1\% \pm 0.4\%$ (if the inter-supermodule regions are excluded) while the average over the whole phi range is $26.5 \pm 0.4\%$.

The average Z efficiency, when both electrons are generated and reconstructed in the barrel calorimeter, is found to be $57.3 \pm 0.2\%$ (where the uncertainties are from the finite number of Monte Carlo events). Half the efficiency loss is caused by the shower-shape requirement, and another quarter by the energy-momentum matching requirement. If events, where at least one electron is reconstructed within the gaps, are removed, the average efficiency is found to be $58.4 \pm 0.2\%$. Assuming that the produced electrons must be homogeneous in ϕ and that

the effects from geometrical gaps can be monitored with some reasonable statistics, it should be straightforward to correct for the detector gaps. Already with the available statistics used for this study, the corrections for the efficiency loss in the gaps can certainly be determined with a relative accuracy smaller than about 25%. This number is estimated from comparing the minimal efficiency in the gap and the efficiency in the non-gap regions.

We conclude that already with a few 100 000 reconstructed Z events, collected at the early stage of the experiment, an efficiency determination with a systematic accuracy of better than 1-2% should be possible. Obviously, with the much larger statistics of a few million Z events, these uncertainties can be further reduced. Once data from the CMS detector becomes available, these cuts can be applied on one electron and varied on the other electron to compare the selection efficiency in data and Monte Carlo simulation. This can be used to further improve the detector simulation and to better access systematic uncertainties.

9.1.2.2 $pp \to W \to e\nu X$ Selection

In order to pass the W $\to$ eν selection, events must have exactly one electron candidate in the barrel fulfilling the requirements described above, and missing transverse energy associated with the neutrino: a cut on the transverse mass of the eν system is applied. The transverse mass $m_T$is defined as follows:

$$m_T = \sqrt{2p_{\mathrm{T}}^{(e)} p_{\mathrm{T}}^{(\nu)} \left(1 - \cos\Delta\phi\right)} \tag{9.1}$$

where $p_{\mathrm{T}}^{(\mathrm{e},\nu)}$ is the (reconstructed) transverse momentum of the electron and the neutrino respectively and $\Delta\phi$ is the azimuthal angle between the electron and the neutrino.

The missing transverse energy can be determined in several ways, for example:

1. From the vector sum of all clusters in the calorimeter
2. From the vector sum of hard objects only

In the electromagnetic calorimeter, the electron transverse energy can be measured accurately. However, the reconstructed transverse missing energy shows a significant bias.

Suspecting that low energy objects (randomly distributed across the detector) are responsible for this bias, we follow the second approach: We select reconstructed jets with a transverse energy above 20 GeV and absolute pseudorapidity less than 2.4 and reconstruct the missing transverse energy only from these jets and the electron. Here we use uncalibrated jets, i.e. whenever we refer to the jet energy we mean raw jet energy.

To study this possibility in more detail, we split our sample into events without jets (as defined in the previous paragraph) and events with one or more jets. Note that in the case of zero accepted jets, only the electron is used to calculate the neutrino transverse energy which is then very close to the electron transverse energy (pointing into opposite directions in ϕ). The transverse mass is equal to twice the electron transverse energy in this case.

No systematic bias is found with this method and the mean value is close to zero. We thus use this method to reconstruct the neutrino transverse energy. The reconstructed W transverse mass is shown in Figure 9.2 right. For the purpose of this analysis and the counting of resonant W events, we require the transverse mass to lie in the interval 60 to 100 GeV/c^2.

We consider two sources of systematic uncertainties here: The uncertainty due to inhomogeneities in the detector geometry and the uncertainty related to the jet veto. We expect that the uncertainty from the reconstruction efficiency as function of the electron azimuthal angle for the efficiency correction will be similar as for the Z selection.

To address the effect of the scale uncertainty of the absolute calibration on the jet definition, we investigated the changes in the selection efficiency when moving the threshold transverse energy for the jet definition. It follows that for a cut on the transverse jet energy at 20 GeV, the efficiency slope is roughly 0.1 % (absolute) per GeV, corresponding to a relative uncertainty of about 0.25% per GeV.

Assuming a jet energy scale uncertainty of 15% at the LHC startup we obtain an efficiency uncertainty of 0.75% relative. For 5% uncertainty in the jet energy scale expected after the final detector calibration), this value reduces to 0.25%.

The efficiency change due to the jet veto can also be estimated directly from $\mathrm{Z} \to \mathrm{e}^+\mathrm{e}^-$ events (applying a jet veto to these events). In the future, this can be done directly from the data recorded with the CMS detector. Thus with the expected large data samples of $\mathrm{Z} \to \mathrm{e}^+\mathrm{e}^-$, remaining differences between data and Monte Carlo can be studied and corrected with very small uncertainties.

9.1.3 W/Z into muons

Simple sets of cuts can be used in CMS to select large statistics samples of $Z \to \mu\mu$ and $W \to \mu\nu$ events with high purity. They are described in detail in Reference [341] and summarised here.

The $Z \to \mu\mu$ selection criteria have been chosen to minimise uncertainties from the muon chamber response and from the matching between the inner tracker and the muon spectrometer. The basic idea is to accept events in which one of the muons is reconstructed as an isolated track in the central tracker detector, even if no associated track in the muon spectrometer is present. This results in a more uniform efficiency as a function of the pseudorapidity, as observed in Figure 9.3 left. From the kinematics point of view only muons with $p_{\mathrm{T}} > 20\,\mathrm{GeV}$ and pseudorapidity $|\eta_\mu| < 2.0$ are considered in the present analysis. A dimuon mass window of $\pm 3\Gamma_Z = 7.5\,\mathrm{GeV}$ around the reconstructed Z mass is used. Figure 9.3 right shows the efficiency of the HLT criteria on the selected sample as a function of the muon pseudo-rapidity. One can clearly observe two regions with smaller efficiency, around $|\eta| \approx 0.25$ and $|\eta| \approx 0.8$, where transitions between two muon wheels take place. The efficiency is dominated by the dimuon component, which represents a unique tool to study the performance of the single-muon subtrigger, which is of relevance for other selections, like $W \to \mu\nu$.

Even if the rate of $W \to \mu\nu$ events is expected to be larger than the $Z \to \mu\mu$ rate by an order of magnitude, the experimental context is more demanding due to a lower trigger efficiency, only moderate transverse missing energy in the event, the absence of a precise mass constraint and a full dependence on tracker and muon spectrometer behaviours. This will lead to larger experimental uncertainties, which can be studied with the $Z \to \mu\mu$ data samples. The selection of $W \to \mu\nu$ events uses the same η cut but a higher p_{T} threshold, $25\,\mathrm{GeV}$, due to the higher threshold for the single-muon trigger. Figure 9.4 shows the transverse invariant mass distribution of the muon-$E_{\mathrm{T}}^{\mathrm{miss}}$ system in $W \to \mu\nu$ events, compared to QCD expectations.

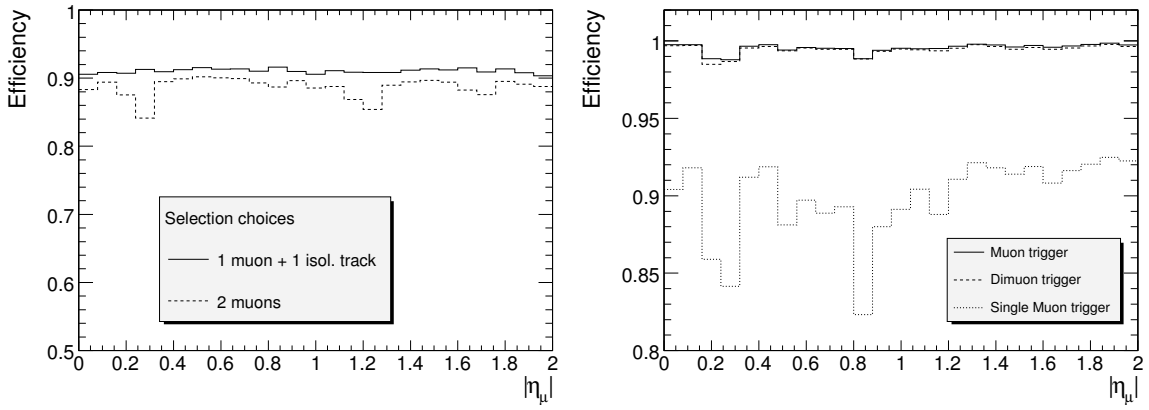

Figure 9.3: Left: Muon efficiency as a function of pseudo-rapidity in the selected $Z \rightarrow \mu\mu$ sample. Two cases are considered: a selection using only muons reconstructed in the muon chambers (dashed histogram) and the selection described in the text (solid histogram), which also accepts isolated tracks in the inner tracker. For this test, no HLT trigger criteria have been applied. Right: HLT efficiency on the selected $Z \rightarrow \mu\mu$ sample as a function of the pseudorapidity of one of the muons. All but the HLT trigger criteria have been applied. The regions at $|\eta| \approx 0.25$ and $|\eta| \approx 0.8$, with a slightly lower trigger efficiency, are visible. The fraction of events triggered by dimuon and single-muon triggers are also shown.

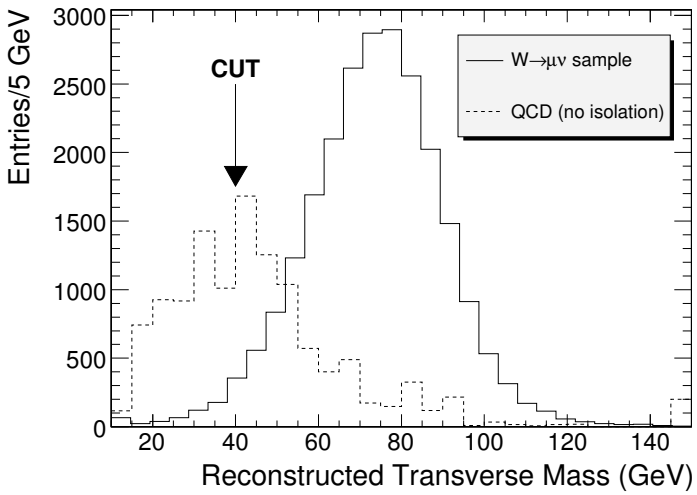

Figure 9.4: Transverse invariant mass reconstructed in $W \rightarrow \mu\nu$ events. In order to observe the shape of the QCD background with more statistics, the HLT muon isolation criteria have not been applied to obtain the plot. The position of the lower cut ($M_{\mu\mu} > 40\,\mathrm{GeV/c^2}$) is indicated with an arrow.

Systematic uncertainties in the determination of $Z \rightarrow \mu\mu$ and $W \rightarrow \mu\nu$ acceptances are summarised in Tables 9.1 and 9.2. The various sources of uncertainties are discussed in detail in Reference [341]. Most of them are evaluated for a CMS detector calibrated with $1\,\text{fb}^{-1}$. The experimental components are well under control in the case of the $Z \rightarrow \mu\mu$ selection, with the limited knowledge on the track efficiency as the dominant source. In the $W \rightarrow \mu\nu$ case, many of them contribute at a similar level, with $E_{\text{T}}^{\text{miss}}$ providing the largest uncertainty. Concerning theoretical sources, the boson p_{T} uncertainties are the dominant contribution. They are estimated from a comparison between LO and NLO CMS simulations using MC@NLO as event generator [342], as shown in Figure 9.5.

Table 9.1: Relative systematic uncertainties on the acceptance for the $Z \rightarrow \mu\mu$ sample.

Source	Uncertainty (%)
Tracker efficiency	1
Magnetic field knowledge	0.03
Tracker alignment	0.14
Trigger efficiency	0.2
Jet energy scale uncertainties	0.35
Pile-up effects	0.30
Underlying event	0.21
Total exp.	1.1
PDF choice (CTEQ61 sets)	0.7
ISR treatment	0.18
p_{T} effects (LO to NLO)	1.83
Total PDF/ISR/NLO	2.0
Total	2.3

Table 9.2: Relative systematic uncertainties on the acceptance for the $W \rightarrow \mu\nu$ sample.

Source	Uncertainty (%)
Tracker efficiency	0.5
Muon efficiency	1
Magnetic field knowledge	0.05
Tracker alignment	0.84
Trigger efficiency	1.0
Transverse missing energy	1.33
Pile-up effects	0.32
Underlying event	0.24
Total exp.	2.2
PDF choice (CTEQ61 sets)	0.9
ISR treatment	0.24
p_{T} effects (LO to NLO)	2.29
Total PDF/ISR/NLO	2.5
Total	3.3

The results of the study can be summarised in terms of cross section measurement accuracies, for $1\,\text{fb}^{-1}$ of integrated luminosity, as follows: $\Delta\sigma/\sigma(pp \rightarrow Z + X \rightarrow \mu\mu + X) =$

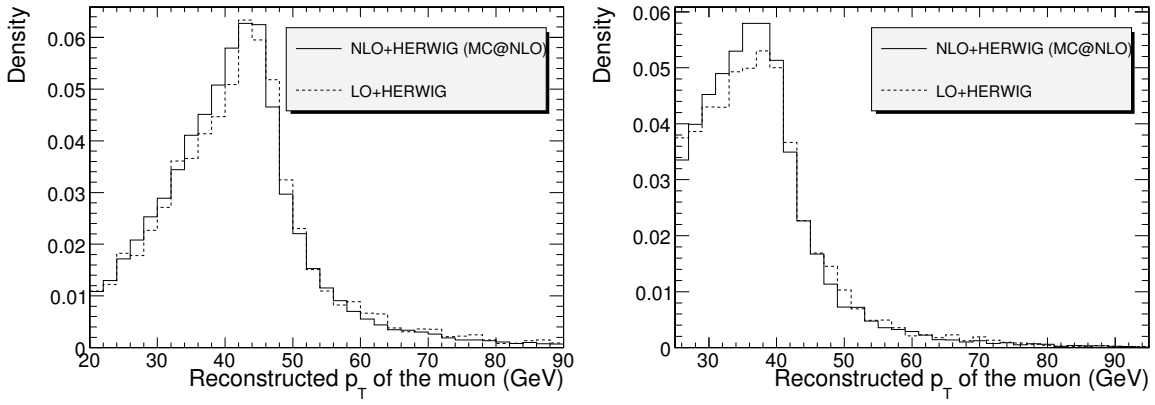

Figure 9.5: Left: Comparison between LO and NLO predictions for the muon p_{T} distribution in $Z \to \mu\mu$ selected events. Both histograms have been normalised to the total number of events generated in the fiducial volume: $|\eta_\mu| < 2.5$, $p_{T\mu}^{max} > 20\,\mathrm{GeV/c}$, $p_{T\mu}^{min} > 10\,\mathrm{GeV/c}$ and $M_Z - 6\Gamma_Z < M_{\mu\mu} < M_Z + 6\Gamma_Z$ Right: Comparison between LO and NLO predictions for the muon p_{T} distribution in $W \to \mu\nu$ selected events. Both histograms have been normalised to the total number of events generated in the fiducial volume: $|\eta_\mu| < 2.5$.

$0.13\ (stat.) \pm 2.3\ (syst.) \pm 10\ (lumi)\ \%$ and $\Delta\sigma/\sigma(pp \to W + X \to \mu\nu + X) = 0.04\ (stat.) \pm 3.3\ (syst.) \pm 10\ (lumi)\%$, where luminosity represents the dominant uncertainty which will eventually decrease to 5% with more integrated luminosity. QCD backgrounds seem to be under control, even if final checks with data will be necessary to determine the level of background with more precision.

Therefore, rates within the fiducial volume of the detector can be determined with high accuracy, even for the first stages of the LHC ($\approx 2.3\%$ for $Z \to \mu\mu$ and $\approx 3.3\%$ for $W \to \mu\nu$). These uncertainties will be significantly reduced with the use of the next generation of NLO Monte Carlos and final detector calibrations, and allow these reactions to be used to determine the luminosity.

9.1.4 Parton distribution functions and parton luminosities

The production of inclusive W and Z events is theoretically well understood and the couplings to quarks and leptons have been measured with accuracies of 1% or better. Thus, it follows from the previous sections that a precise counting of $W \to e\nu, \mu\nu$ and $Z \to ee, \mu\mu$ events is equivalent to a precise measurement of the quantity

$$\int_{q,\bar{q}\ partons} dx_1 dx_2 \sigma_{q\bar{q}\to W,Z} \times L_{pp} \times PDF(x_1, x_2, Q^2), \tag{9.2}$$

where L_{pp} is the LHC integrated luminosity, $\sigma_{q\bar{q}\to W,Z}$ is the cross section for inclusive W or Z production at the partonic level and $PDF(x_1, x_2, Q^2)$ denotes the probability to produce quarks and anti-quarks with proton fractions x_1 and x_2 at a scale Q^2. The prospect studies of Reference [341], summarised in Table 9.3, show that uncertainties on the parton distribution functions (PDF) have a relatively small influence on the experimental acceptance for the rates, but a large effect on the global rate expectations.

We conclude from Table 9.3 that a comparison between theory and experiment with a $6 - 7\%$ accuracy is possible. This comparison provides a measurement of the integrated luminosity

Table 9.3: Estimated uncertainties in the rate and in the acceptance for the $pp \to Z + X \to \mu\mu + X$ and $pp \to W + X \to \mu\nu + X$ processes. The global rate is referred to the fiducial volumes used in Reference [341], which include a pseudorapidity cut of $|\eta_\mu| < 2.5$.

	$Z \to \mu\mu$	$W \to \mu\nu$
Global rate uncertainty (%)	$^{+5.8}_{-7.9}$	$^{+5.6}_{-7.4}$
Acceptance uncertainty (%)	$^{+0.4}_{-0.7}$	$^{+0.6}_{-0.9}$

L_{pp} with a similar level of precision. The small theoretical uncertainties on the experimentally measured rate (from the acceptance uncertainty) allow precise measurements of cross section ratios, such as $\sigma(pp \to ZZ + X)/\sigma(pp \to Z + X)$, in which PDF and luminosity uncertainties cancel. Current studies within theoretical and experimental communities [343] aim to a further reduction of uncertainties associated to PDFs. Finally, PDF validity tests and further reductions in the acceptance uncertainty (below the percent level) will require dedicated studies of the lepton rapidity distributions observed in data, like those suggested in Reference [344].

9.2 Muon pairs from the Drell-Yan process

9.2.1 Introduction

In the Standard Model, the production of lepton pairs in hadron-hadron collisions, the Drell-Yan (DY) process [345], is described by s-channel exchange of photons or Z bosons. The parton cross section in the lepton-pair centre-of-mass system has the form:

$$\frac{d\sigma}{d\Omega} = \frac{\alpha^2}{4s}[A_0(1 + \cos^2\theta) + A_1 \cos\theta] \tag{9.3}$$

where $\sigma = \frac{4\pi\alpha^2}{3s}A_0$ and $A_{\mathrm{FB}} = \frac{3}{8}\frac{A_1}{A_0}$ are the total cross section and the forward-backward asymmetry, and θ is angle of lepton in the dilepton rest frame with respect to the quark direction. The terms A_0 and A_1 are fully determined by the electroweak couplings of the initial- and final-state fermions. At the Z peak the Z exchange is dominating and the interference term is vanishing. At higher energies both photon and Z exchange contribute and the large value of the forward-backward asymmetry is due to the interference between the neutral currents. Fermion-pair production above the Z pole is a rich search field for new phenomena at present and future high energy colliders. The differential cross section is sensitive to manifestation of new physics from a multi-TeV scale by adding new amplitudes or through their interference with the neutral currents of the SM. At hadron colliders the parton cross sections are folded with the parton density functions (PDF): $pp \to l_1 l_2$

$$\frac{\mathrm{d}^2\sigma}{\mathrm{d}M_{ll}\mathrm{d}y}[pp \to l_1 l_2 + X] \approx \sum_{ij} \left(f_{i/p}(x_1) f_{j/p}(x_2) + (i \leftrightarrow j)\right) \hat{\sigma}\,, \tag{9.4}$$

where $\hat{\sigma}$ is the cross section for the partonic subprocess $ij \to l_1 l_2$, $M_{ll} = \sqrt{\tau s} = \sqrt{\hat{s}}$ the mass of the lepton-pair system, y the rapidity of the lepton pair, $x_1 = \sqrt{\tau}e^{y}$ and $x_2 = \sqrt{\tau}e^{-y}$ the parton momentum fractions, and $f_{i/p(\bar{p})}(x_i)$ the probability to find a parton i with momentum fraction x_i in the proton.

Table 9.4: x_1 and x_2 for different masses and rapidities.

y	0	2	4	0	2	4	0	2	4
	M = 91.2 GeV/c^2			M = 200 GeV/c^2			M = 1000 GeV/c^2		
x_1	0.0065	0.0481	0.3557	0.0143	0.1056	0.7800	0.0714	0.5278	-
x_2	0.0065	0.0009	0.0001	0.0143	0.0019	0.0003	0.0714	0.0097	-

The total cross section and the forward-backward asymmetry are function of observables which are well measured experimentally for final states containing e^+e^- or $\mu^+\mu^-$: the invariant mass and the rapidity of the final-state lepton pair. This allows to reconstruct the centre-of-mass energy of the initial partons, even if their flavours are unknown. For a ($x_1 \geq x_2$) pair of partons we have 4 combinations of *up*- or *down*-type quarks initiating the interaction: $u\bar{u}, \bar{u}u, d\bar{d}, \bar{d}d$. In pp collisions the anti-quarks come always from the sea and the quarks can have valence or sea origin. The x-range probed depends on the mass and rapidity of the lepton pair as shown in Table 9.4.

The results presented here extend the studies for the LHC SM workshop (see [157] and references therein), using more data and the CMS full detector simulation and reconstruction. More details can be found in [346].

9.2.2 Cross section measurements

Simulation of Drell-Yan events in proton-proton collisions at 14 TeV centre-of-mass energy is performed with PYTHIA 6.217 using the CTEQ5L parton distribution functions. The possible contributions from higher-order terms in the dimuon production cross section are taken into account by using a K factor of 1.3 as calculated with the program PHOZPRMS [347]. Eleven samples of 10 000 events each with different cut-off values on the dimuon invariant mass are generated: $M_{inv} \geq$ 0.2, 0.5, 1, 1.5, 2, 2.5, 3, 3.5, 4, 4.5, 5 TeV/c^2. Only events with at least two muons in the pseudorapidity range $|\eta| \leq 2.5$, with transverse momentum $p_T \geq 7$ GeV/c are preselected. No cuts on isolation of muons are made at the pre-selection stage. The total efficiency for dimuon pre-selection, ε, is about 87% for a mass of 1 TeV$/c^2$ and 96% for a mass of 5 TeV/c^2. To simulate the detector geometry, materials and particle propagation inside the detector, the GEANT 4-based simulation of the CMS detector is used.

The trigger simulation is based on the on-line reconstruction algorithms. Events are selected by the single- and double-muon triggers. This means that at least one muon candidate is within pseudorapidity region $|\eta| \leq 2.1$. The total efficiency of triggering including reconstruction and trigger selection efficiency is 98 % at 1 TeV. There is significant decrease in trigger efficiency after applying calorimeter isolation cuts (down by 15 %). The tracker isolation practically does not affect the trigger efficiency. Thus the additional cuts on calorimeter and tracker isolation of muon tracks are not applied in this analysis.

The off-line muon reconstruction algorithm is applied only to events which have passed trigger selection. At the off-line level two muons inside the CMS acceptance $|\eta| \leq 2.4$ are required. The overall efficiency of the full reconstruction procedure taking into account trigger and off-line reconstruction inefficiency is between 97% and 93% for a mass range of 0.2 to 5 TeV/c^2, as shown in Figure 9.6 left. In the case of an ideal detector the mass resolution smearing for fully-reconstructed events is between 1.8% and 6% for the same mass range, Figure 9.6 right. The effect of misalignment on the mass resolution varies from 1.1% up to 2.3% (1.3%) for the *First Data* (*Long Term*) scenarios at the Z and from 5% up to 25% (6%) for

3 TeV/c^2.

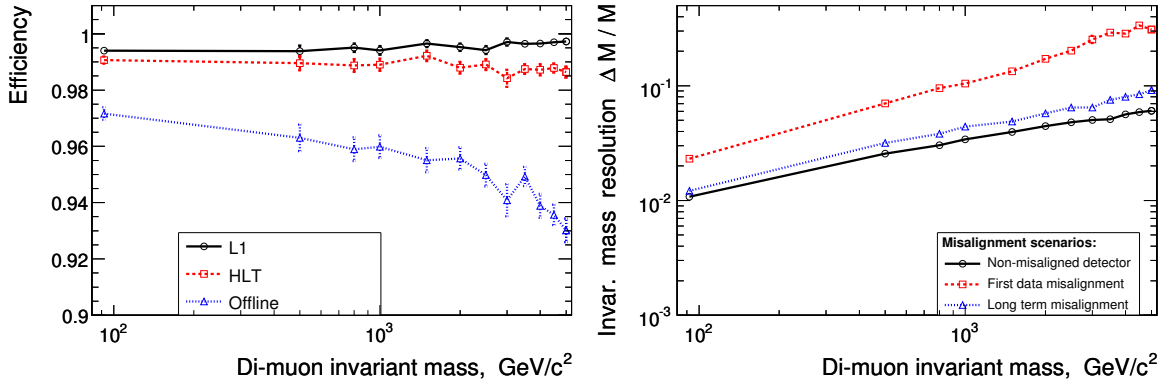

Figure 9.6: Left: dimuon reconstruction efficiency, and right: invariant mass resolution; both as function of the invariant mass cut.

The cross sections of Drell-Yan production for the simulated CMS runs are shown in Table 9.5. The non-reducible backgrounds considered are vector boson pair production ZZ, WZ, WW, $t\bar{t}$ production etc. The simulation and pre-selection of background events is done with the same cuts as for the signal above. In the SM the expected leading-order cross section of these events is negligible in comparison with the Drell-Yan one, see Table 9.5.

Table 9.5: Leading-order cross sections of Drell-Yan, preselected Drell-Yan, dibosons (ZZ, ZW, WW) and $t\bar{t}$ events in fb. The CTEQ5L parton distributions are used.

$M_{\mu^+\mu^-}$, TeV/c^2	≥ 1.0	≥ 1.5	≥ 2.0	≥ 2.5	≥ 3.0	≥ 4.0
Drell-Yan	6.61	1.04	$2.39 \cdot 10^{-1}$	$6.53 \cdot 10^{-2}$	$1.97 \cdot 10^{-2}$	$2.09 \cdot 10^{-3}$
Pre-sel. D-Y	5.77	$9.53 \cdot 10^{-1}$	$2.24 \cdot 10^{-1}$	$6.14 \cdot 10^{-2}$	$1.87 \cdot 10^{-2}$	$2.00 \cdot 10^{-3}$
Dibosons	$2.59 \cdot 10^{-4}$	$1.51 \cdot 10^{-4}$	$5.6 \cdot 10^{-5}$	$2.26 \cdot 10^{-5}$	$9.06 \cdot 10^{-6}$	$1.66 \cdot 10^{-6}$
$t\bar{t}$	$2.88 \cdot 10^{-4}$	$2.58 \cdot 10^{-4}$	$1.55 \cdot 10^{-4}$	$7.02 \cdot 10^{-5}$	$2.93 \cdot 10^{-5}$	$3.65 \cdot 10^{-6}$

The $\tau\tau$ background (from τ decaying to μ and neutrinos) is 0.8 % at the Z pole and 0.7 % for masses above 1 TeV/c^2. The background from Drell-Yan production of $q\bar{q}$ pairs (mostly semi-leptonic b or c decays) is 0.3 % at the Z pole without applying any isolation cuts and below 0.1 % for masses above 1 TeV/c^2. The other background sources are negligible. If the need arises they can be further suppressed by acoplanarity and isolation cuts in the tracker.

The main experimental systematic effects in the cross section measurement arise from the total muon inefficiency and momentum resolution. The latter is very important at high mass as smearing from lower masses from the steeply falling Drell-Yan spectrum can contaminate the high mass measurements, especially if the tails of the momentum resolution are not under control. The main sources of systematic uncertainties on the momentum resolution come from the alignment of the muon chambers and the central tracker, both at start-up and high luminosity.

The statistical errors for 1, 10 and 100 fb^{-1} runs, the systematic uncertainty due to smearing in the detector and from theory side are given in Table 9.6. The modification of the measured cross section due to uncertainty of the mass resolution does not exceed 2.9% which is reached

Table 9.6: Relative errors of the Drell-Yan muon pairs cross section measurements in the fiducial volume.

$M_{\mu^+\mu^-}$, TeV/c^2	Detector smearing	Statistical 1 fb^{-1}	Statistical 10 fb^{-1}	Statistical 100 fb^{-1}	Theor. Syst.
≥ 0.2	$8 \cdot 10^{-4}$	0.025	0.008	0.0026	0.058
≥ 0.5	0.0014	0.11	0.035	0.011	0.037
≥ 1.0	0.0049	0.37	0.11	0.037	0.063
≥ 2.0	0.017		0.56	0.18	0.097
≥ 3.0	0.029			0.64	0.134

for a mass of 3 TeV/c^2, see Table 9.6. This has been estimated by applying an additional smearing to the dimuon mass (see [98, 346]). The misalignment does not affect the efficiency of dimuon reconstruction for any masses [98]. Taking into account the trigger efficiency changes from 98.5% to 97% for masses from 0.2 to 5 TeV/c^2, very conservatively we may assign half of this change with mass, i.e., 0.75%, as a systematic uncertainty.

An important ingredient in the cross section measurement is the precise determination of the luminosity. A promising possibility is to go directly to the parton luminosity [344] by using the $W^{\pm}$ (Z) production of single (pair) leptons. New estimates show that in this way the systematic error on $\sigma_{DY}^{high\ Q^2}$ *relative* to σ_Z can be reduced to $\approx 5 - 12\%$ [348].

On the theory side we consider several sources of systematic uncertainties. Higher order QCD corrections are often taken into account with K-factor of 1.3 as calculated with the program PHOZPRMS [347]. It is expected that the total value of additional NNLO contributions does not exceed 8% .

A full-scale analysis of experimental data (comparison data with theory, taking into account acceptance corrections for precise measurement of σ and A_{FB} at large centre-of-mass energies $\hat{s}$) requires good knowledge of the different types of genuine electroweak (EW) radiative corrections to the DY process: vertex, propagator, EW boxes. A complete one-loop parton cross section calculation has been included in [157] and confirmed in [349]. The EW corrections change the cross section by 10-20%. The calculation [104] of the weak radiative corrections to the Drell-Yan processes due to additional heavy bosons contributions shows that these corrections are about 2.9% to 9.7% for mass region between 0.2 TeV/c^2 and 5 TeV/c^2.

The phenomenological origin of PDF gives one additional systematic error. First of all, estimates of cross section obtained by using different sets of structure functions do not give exactly the same values. The results vary within ± 7 % for $M_{ll} \geq 1$ TeV/c^2. The internal PDF uncertainties are estimated using the LHAPDF library [94, 350]. The PDF-dependence of the acceptance efficiency is estimated by using the PDF sets CTEQ5L, CTEQ6L and MRST2001E. The changes in the acceptance efficiency are up to 0.5 %. The ambiguity in the acceptance efficiency due to internal PDF uncertainties is larger, but less than 1.4 % for any mass region.

The summary of the estimated systematic uncertainties as function of the dilepton mass is given in Figure 9.7. The CMS experiment has excellent potential to measure the cross section for dimuon pairs up to the highest masses that will be accessible at the LHC, and to test the Standard Model up to very high momentum transfers in a new and unexplored energy range. Current uncertainties from theory are larger than the experimental uncertainties. The

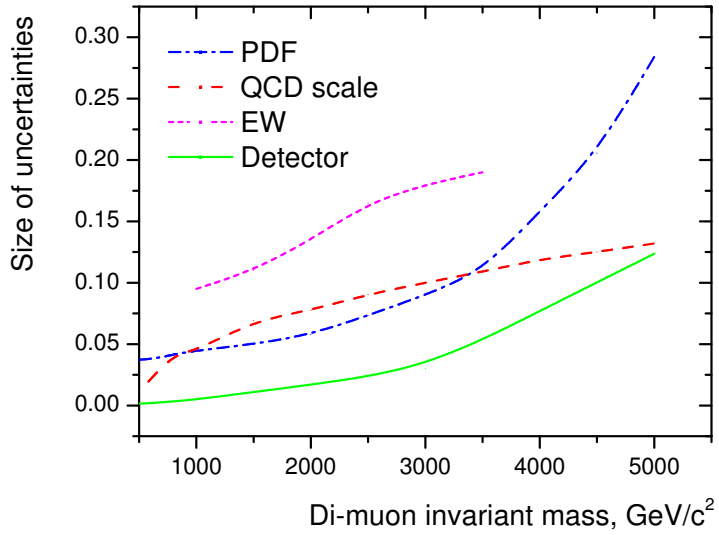

Figure 9.7: Size of the EW corrections and the cross section uncertainties from PDFs, hard process scale and detector understanding as a function of the dimuon invariant mass cut.

statistical errors will dominate for invariant masses larger than 2 TeV/c^2 even for 100 fb^{-1}.

9.2.3 Prospects on the measurement of the forward-backward asymmetry

To measure the forward-backward asymmetry we need the original quark and anti-quark directions of the initiating partons, but these are not known in the case of pp experiments, where the initial state is symmetric. In Ref. [95, 111] it is shown that it is possible to approximate the quark direction with the boost direction of the dimuon system with respect to the beam axis. This is due to the fact that the valence quarks have on average larger momentum than the sea anti-quarks, and therefore the dimuon boost direction approximates the quark direction. The most unambiguous tagging occurs for large dimuon rapidity.

The approximation of the original quark direction for pp collisions leads to a flattening out of the original asymmetry (≈ 0.61 for Drell-Yan events) by a factor of almost 2. However, using multi-dimensional fits [110] or reweighting techniques depending on the mistag and acceptance which are under development, we can measure the original asymmetry.

The accuracy of asymmetry measurements depends on:

- statistical uncertainty which grows with rising mass cut value, as the number of events for integrated luminosity of e.g. $\int \mathcal{L}\,dt = 100\,\text{fb}^{-1}$ decreases with mass
- systematic uncertainty from the variation of the mistag probabilities for various PDF sets, typically below 10 %.

We expect the systematic uncertainty to dominate the statistical one for integrated luminosity of $\int \mathcal{L}\,dt = 100\,\text{fb}^{-1}$ and dimuon masses around 500 GeV/c^2, while the statistical one to be more important for dimuon mass cuts above 1000 GeV/c^2.

9.3 Determination of the W mass

9.3.1 Introduction

The precise measurement of the mass of the W boson constitutes an important consistency check of the Standard Model and, together with the top quark mass, is sensitive to supersymmetric corrections. Such a precision measurement of the W mass at the LHC becomes feasible because a huge sample of data available at the LHC will guarantee a nearly negligible statistical uncertainty and a good control of the systematic effects. Extrapolating from traditional approaches based on the reconstruction of the transverse mass $m_T = \sqrt{2p_{\mathrm{T}}^{l}p_{\mathrm{T}}^{\nu}(1-\cos(p_{\mathrm{T}}^{l},p_{\mathrm{T}}^{\nu}))}$ in leptonic W decays, the most relevant contributions to the systematic uncertainties come from the lepton energy or momentum scale, the lepton energy or momentum resolution, the modelling of the system recoiling against the W boson, the parton distribution functions, the W intrinsic width, from radiative decays and from backgrounds. To accomplish a competitive measurement of the W boson mass, new strategies must be considered [351]. The most promising one consists in predicting the distribution of experimental observables sensitive to the W mass, such as the transverse momentum of the charged lepton (p_{T}^{l}) and the transverse mass of the boson from the corresponding distribution measured in Z boson decays into two charged leptons. The concept of transverse mass measurement can be applied to Z boson events by regarding one of the reconstructed leptons as missing energy. The theoretical description of both decays is very similar and the resulting distributions in transverse mass are comparable for a wide range in kinematics.

The advantage of this approach, conceptually discussed in [352], is that most of the experimental and theoretical uncertainties, being common between W and Z, cancel in the comparison, leading to a global reduction of the systematic uncertainty. The drawback is a larger statistical uncertainty due to the smaller production rate of Z bosons decaying to charged leptons. Yet a statistical precision of order 10 MeV/c^2 and 30 MeV/c^2 for an integrated luminosity of 10 fb^{-1} and 1 fb^{-1} respectively is anticipated. In order not to be limited by statistics, the analyses are performed using large data samples produced with the fast simulation of the CMS experiment [11]. Smaller samples of fully simulated events are used for cross checks.

Two different ways to relate Z to W boson events are considered. One is based on the comparison of the same experimental observables in W- and Z-events scaled to the boson masses. The sensitivity of this method, which can take advantage of the precision calculation of the theoretical ratio of the W and Z boson differential production cross-sections, is fully addressed in the analysis of transverse energy distribution of the electrons from $W \to e\nu$ decays. An alternative approach considered in the analysis of $W \to \mu\nu$ events consists of predicting W boson distributions from Z-events by means of kinematic transformations of measured Z events, parameterised as a function of the boson masses and widths. This more phenomenological approach is exploited in the analysis of the transverse mass distributions, and relies less on the theoretical prediction of the boson p_{T}.

9.3.2 Event selections

In order to obtain a clean signal of $W \to \mathrm{l}\nu$ decays, events that passed the High Level Trigger (HLT) for single leptons are required to satisfy the following selection cuts: one isolated muon with $p_{\mathrm{T}} > 25\,\mathrm{GeV/c}$ within the pseudo-rapidity region $|\eta| < 2.3$ or one isolated electron with $p_{\mathrm{T}} > 25\,\mathrm{GeV/c}$ and within $|\eta| < 2.4$; missing transverse energy $E_{\mathrm{T}}^{\mathrm{miss}} > 25\,\mathrm{GeV}$;

no jets in the event with $p_{\mathrm{T}jet} > 30\,\mathrm{GeV/c}$; the transverse momentum of the system recoiling against W has to be lower than 20 GeV/c, measured from the lepton p_{T} and the missing transverse energy.

The difference in minimum p_{T} of the charged lepton is determined by the single lepton trigger threshold. The last two selection cuts are intended to select W bosons produced with a small transverse momentum. The selection efficiency is about 15% for the electron channel and 25% for the muon channel, with a background at the percent level, dominated by leptonic Z decays with one lepton outside the acceptance, as shown in Figure 9.8.

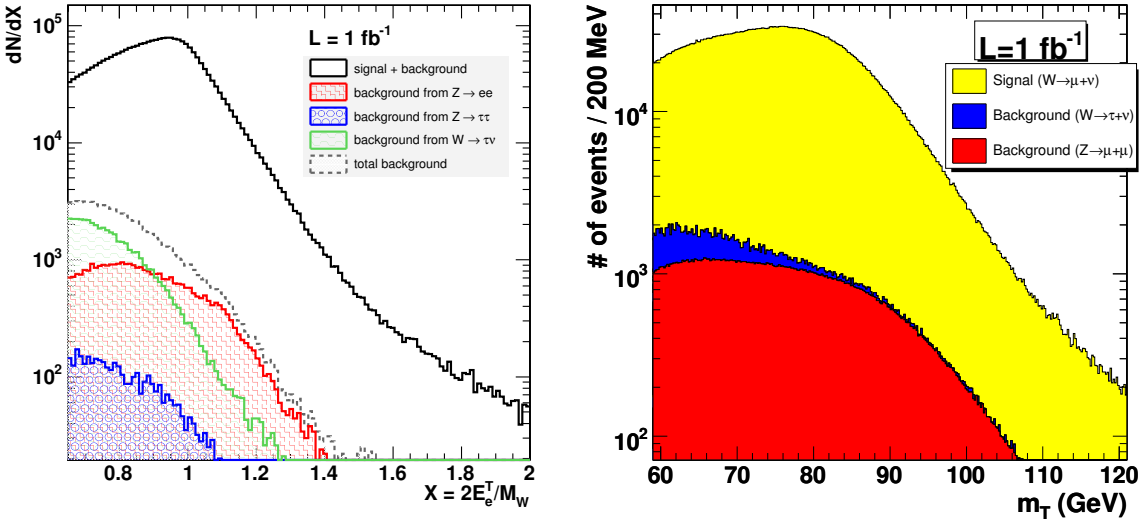

Figure 9.8: W events and main backgrounds for $1\,\mathrm{fb}^{-1}$. Left: Electron scaled transverse energy distribution in $W \to e\nu$ decays and the backgrounds from $Z \to e^+e^-$, from $Z \to \tau^+\tau^-$ and from $W \to \tau\nu$ for $1\,\mathrm{fb}^{-1}$. Right: Transverse mass distribution in the muon channel with the fractions of $Z^0/\gamma^* \to \mu^+\mu^-$ (red/grey) $W \to \tau\nu$ (blue/dark), and W$\to \mu\nu$ (yellow/light) events.

Z events used to predict the W distribution are also selected from the sample of events passing the HLT for single leptons. Z candidates contain a pair of identified charged leptons consistent with the Z mass hypothesis [351]. One of the two leptons, randomly chosen, is removed from the event to mimic a W decay. The same selections discussed above are then applied, with the cut values on the lepton quantities (minimum lepton p_{T} and event missing transverse energy) scaled by the ratio M_Z/M_W. This choice is intended to minimise kinematic and acceptance differences in Z and W events and thus the theoretical uncertainties implied by the above mentioned approaches.

9.3.3 $W \to e\nu$

The analysis strategy is based on the prediction of the experimental distribution of the electron transverse energy in W events scaled to the boson mass from the corresponding distribution measured for Z bosons decaying into e^+e^- pairs, along with the theoretical ratio between the W and Z cross-sections, calculated at a fixed perturbative order. Ideally, the differential cross section for the W boson can be predicted from the one measured for Z boson by scaling the lepton transverse momenta with the boson masses, $p_{\mathrm{T}}^{\mathrm{lept,Z}} = M_Z/M_W p_{\mathrm{T}}^{\mathrm{lept,W}}$,

as:

$$\left.\frac{d\sigma^W}{dp_{\mathrm{T}}^{\mathrm{lept,W}}}\right|_{pred} = \frac{M_Z}{M_W} R(X) \left.\frac{d\sigma^Z}{dp_{\mathrm{T}}^{\mathrm{lept,Z}}}\left(p_{\mathrm{T}}^{\mathrm{lept,Z}} = \frac{M_Z}{M_W} p_{\mathrm{T}}^{\mathrm{lept,W}}\right)\right|_{meas}, \tag{9.5}$$

where $R(X) = \frac{d\sigma^W}{dX^W} / \frac{d\sigma^Z}{dX^Z}$ is the ratio, deduced from theoretical calculations, between the differential cross sections in terms of the scaled variable $X^V = \frac{p_{\mathrm{T}}^{\mathrm{lept},V}}{M_V}$, with V=W,Z. The parameter M_W can be extracted by fitting this prediction to the distribution for W events observed in the experiment. In practice, additional corrections to $R(X)$ are needed to account for the acceptance to Z and W events and for the experimental resolution. This calls for a detailed understanding of the detector response by means of Monte Carlo simulations compared to control samples. Clearly, the definition of $R(X)$ is the most critical aspect and must include both detector effects and theoretical predictions.

The results for 1 fb^{-1} of integrated luminosity using the technique just described are shown in Figure 9.9. The statistical precision of the method is determined from the resulting χ^2 distribution. The evaluation of the systematic uncertainties affecting the measurement of the W mass is performed by determining the distortions implied by the different systematic effects mentioned above. The effects of instrumental origin have been studied by fixing $R(X)$ to the theoretical prediction exactly describing the samples of generated events (i.e. an exact knowledge of the theory is assumed) and by introducing distortions and biases in the detector response. The resulting shift in M_W is assumed as the systematic uncertainty associated to the effect. The detector response to electrons, the largest source of systematic uncertainty of instrumental origin with this method, can be determined with the required precision from $Z \to ee$ events.

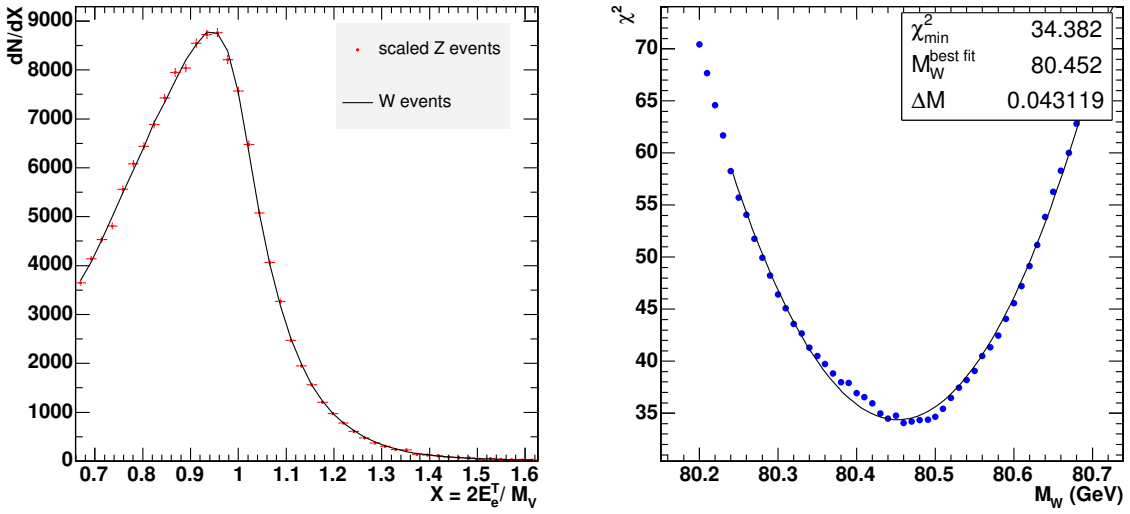

Figure 9.9: Comparison of the scaled electron E_T spectra for Z (dots) and W boson (line) events (left) and χ^2 dependence on M_W (right) for 1 fb^{-1} of integrated luminosity.

The prediction of the lepton transverse spectrum is plagued by large radiative QCD corrections. Yet, in the method adopted, large cancellations occur and $R(X)$ can be reliably predicted. The uncertainty related to the missing orders in the perturbative expansion can be quantified by the dependence of the available NLO prediction on the choice of the renormalisation and factorisation scales. A conservative figure of 30 MeV/c^2 for the mass uncertainty

is deduced. This will become the dominant error at 10 fb^{-1}. Yet the reduction of this error by extending the calculation one order higher in α_S is technically feasible [352].

9.3.4 $W \to \mu\nu$

As a complementary method, the transverse mass distribution of W events in the muon channel is modelled from Z$\to \mu^+\mu^-$ events by a kinematic transformation. In the rest frame of the Z boson, the lepton momenta are scaled such that their invariant mass distribution represents that of the W boson [351]. After removing one randomly chosen muon to mimic a neutrino, the whole system is boosted back into the detector frame, thus obtaining a template for the expected distribution of W events, which depends on the W and Z boson masses and widths as parameters. By iterating the procedure for different W boson masses, the best agreement with the observed transverse mass distribution in W events is determined using a χ^2 criterion. In practice, weighting factors take into account unavoidable differences between the W and Z samples, such as the acceptance for the second lepton, photon radiation, and differences in η and p_{T} of W and Z bosons. Thus perfect agreement of the distributions at the nominal W mass and for the simulated detector is ensured, while systematic effects are studied by introducing distortions of experimental or theoretical origin. The resulting shifts in the extracted W mass are taken as the related systematic uncertainties.

The dominant systematic error arises from scale and resolution uncertainties in the missing energy determined from the calorimeters. These can be controlled by using the Z sample, where the boson p_{T} can be measured from the two charged leptons, as is shown in Figure 9.10. The observed differences of 2% on the scale and 5% on the resolution are taken as the systematic uncertainties.

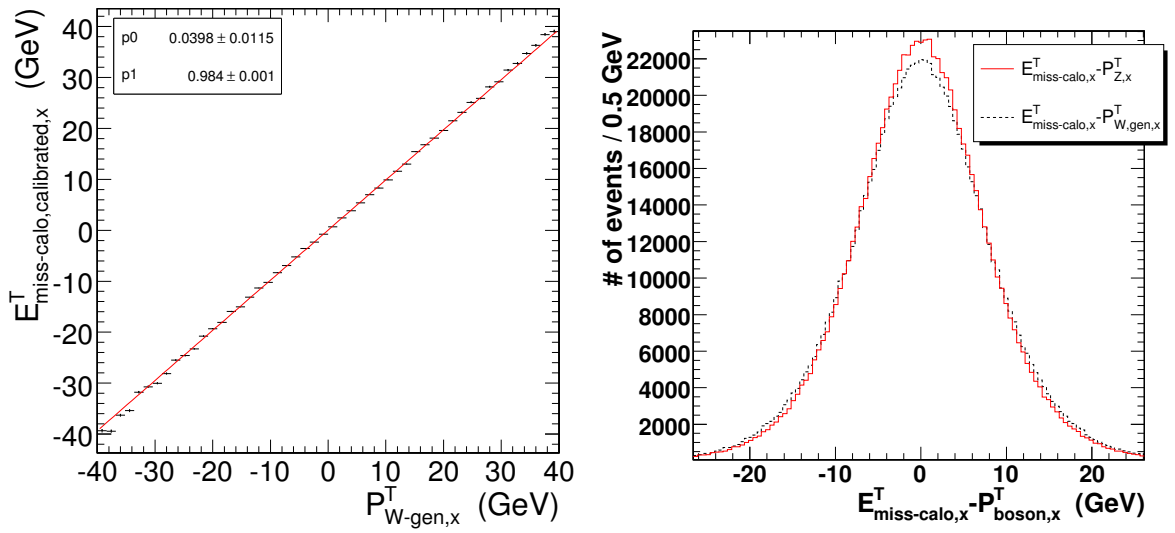

Figure 9.10: Left: x-component of the calibrated missing transverse energy in the calorimeters using the reconstructed muon p_{T} in Z events, as a function of the transverse W boson momentum at generator level. The slope of a fitted straight line is 0.98. Right: Difference between the reconstructed missing energy in the calorimeters and the measured muon p_{T} in Z events (red/grey line) or the W boson p_{T} at generator level (black dashed line). The RMS of the distribution is 8.15 GeV for Z events and 8.65 GeV for W events.

9.3.5 Expected precision and systematic uncertainties

The expected size of various detector effects for the early detector operation, after the analysis of an initial integrated luminosity of 1 fb^{-1}, and for a better detector understanding expected after employing an integrated luminosity of 10 fb^{-1}, is shown in Table 9.7 for the scaled p_{T}-lepton method applied to the electron channel, and for the muon channel using the transformation method.

Table 9.7: Expected systematic uncertainties on M_{W} for the scaled E^T-lepton method with electrons (upper part) and for the Z transformation method applied to the muon channel (lower part). The first column lists the systematic effect considered, the second and third columns show the assumed detector uncertainty for an initial integrated luminosity of 1 fb^{-1} and the resulting uncertainty on M_W. The last two columns show the extrapolation to an integrated luminosity of 10 fb^{-1}, when the detector understanding is assumed to have significantly improved.

Source of uncertainty	uncertainty with 1 fb^{-1}	ΔM_W [MeV/c^2] with 1 fb^{-1}	uncertainty with 10 fb^{-1}	ΔM_W [MeV/c^2] with 10 fb^{-1}
scaled lepton-p_{T} method applied to W$\rightarrow e\nu$				
statistics		**40**		15
background	10%	10	2%	2
electron energy scale	0.25%	10	0.05%	2
scale linearity	0.00006/ GeV	30	<0.00002/ GeV	<10
energy resolution	8%	5	3%	2
MET scale	2%	15	<1.5%	<10
MET resolution	5%	9	<2.5%	< 5
recoil system	2%	15	<1.5%	<10
total instrumental		**40**		**<20**
PDF uncertainties		20		<10
Γ_W		15		<15
$p_{\mathrm{T}}^{\mathrm{W}}$		30		30 (or NNLO)
transformation method applied to W$\rightarrow \mu\nu$				
statistics		**40**		15
background	10%	4	2%	negligible
momentum scale	0.1%	14	<0.1%	<10
$1/p^T$ resolution	10%	30	<3%	<10
acceptance definition	η-resol.	19	$< \sigma_\eta$	<10
calorimeter $E_{\mathrm{T}}^{\mathrm{miss}}$, scale	2%	38	$\leq$1%	<20
calorimeter $E_{\mathrm{T}}^{\mathrm{miss}}$, resolution	5%	30	<3%	<18
detector alignment		12	–	negligible
total instrumental		**64**		**<30**
PDF uncertainties		$\approx$20		<10
Γ_W		10		< 10

The measurements of the W mass by means of $W \rightarrow e\nu$ and $W \rightarrow \mu\nu$ decays are largely independent. Common experimental uncertainties arise from the systematics involving the missing transverse energy in the calorimeters.

Based on the estimated systematic errors, it is clear that the scaled p^T-lepton method suffers less from experimental systematic errors than the transformation method. If systematic uncertainties arising from the theoretical prediction of the transverse momenta of the Z and W bosons can be brought to a level of $\approx$ 10 MeV/c^2, the scaled p^T-lepton method is clearly the first choice. Using the scaled p_{T}-lepton method in the muon channel leads to a better

statistical precision of 30 MeV/c^2 for 1 fb^{-1} due to the higher acceptance for muons compared to electrons. The total instrumental uncertainty of the p_{T}-lepton method applied to the muon channel is estimated from the findings in the electron channel and amounts to about 25 MeV/c^2 for the initial measurement with an integrated luminosity of 1 fb^{-1}. Uncertainties due to the recoil modelling are fully correlated with the electron channel. The component of the experimental error in common with the electrons amounts to about 20 MeV/c^2. Clearly, all theoretical uncertainties are of similar size and also correlated between the electron and muon channels.

The transformation method has the advantage of providing templates for observables in W events from measured observables in Z events. In particular, the measurement of the transverse momentum of Z bosons and the cross checks on the modelling of the missing energy are of vital importance to quantify systematic uncertainties.

The combination of the electron and muon channels brings the statistical uncertainty to a final precision of better than 10 MeV/c^2 for an integrated luminosity of 10 fb^{-1}, and a systematic uncertainty of instrumental origin below 20 MeV/c^2 should be within reach.

9.4 Multi-boson production

9.4.1 Introduction

The study of multiple gauge-boson production at the TeV scale constitutes a unique opportunity to test the Standard Model of Electroweak interactions at the highest possible energies. The production of $W^{\pm}$ Z^0 and $W^{\pm}\gamma$ events at the LHC probes the triple gauge-boson couplings and therefore the non-Abelian gauge symmetry of the Standard Model. On the other hand, no neutral gauge-boson couplings exist in the Standard Model, thus anomalies in Z^0 Z^0 and $Z^0\gamma$ production, hinting at large s-channel contributions, could be the first indirect manifestation of New Physics. In the following, the selections of $W^{\pm}$ Z^0 and Z^0 Z^0 events are described, their signal-over-background ratio discussed and the outlook for an early measurement of multiple gauge-boson production is assessed. Further details are given in Reference [353].

The multi-lepton final states of multiple gauge-boson production are an important background in the search for New Physics, in particular Supersymmetry. A sound understanding of their production process is therefore needed in the first phase of LHC data-taking before any discovery can be claimed. In particular, Z^0 Z^0 production is an irreducible background to the most-coveted discovery at the LHC: the Standard Model Higgs boson. Its early measurement is therefore important.

The cross sections for multiple gauge-boson production at the LHC are of about 50 pb for the $W^{\pm}$ Z^0 channel and 20 pb for the Z^0 Z^0 channel [157]. These large cross sections and the clean signature of fully-leptonic final states make $W^{\pm}$ Z^0 and Z^0 Z^0 production observable in the early LHC data. Final states where the gauge bosons decay into electrons and muons are considered: $e^{\pm}e^+e^-$, $\mu^{\pm}e^+e^-$, $e^{\pm}\mu^+\mu^-$ and $\mu^{\pm}\mu^+\mu^-$ for $W^{\pm}$ Z^0 production and $e^+e^-e^+e^-$ for the Z^0 Z^0 channel. The competing background processes are the Standard Model production of gauge bosons and top quarks, which also yield leptonic final states.

9.4.2 Signal definition and modelling

Both the $W^{\pm}\,Z^0$ and $Z^0\,Z^0$ analyses focus on on-shell gauge bosons. On-shell production of the $W^{\pm}\,Z^0$ final state proceeds mainly through the s-channel, involving a WWZ triple gauge-boson coupling. Additional contributions from the $W^{\pm}\gamma^*$ final state through a $WW\gamma$ coupling are effectively suppressed by constraining the mass of the observed lepton pair to be compatible with a Z^0 boson. The PYTHIA Monte Carlo generator [24] is used to model $W^{\pm}\,Z^0$ production and subsequent decay into fully-leptonic final states. Gauge-boson decays into tau leptons are also included. These tau leptons are left free to decay into either leptons or hadrons.

Four-electron final-states can originate from $Z^0\,Z^0$ production as well as via either $Z^0\gamma^*$ or $\gamma^*\gamma^*$ production. The requirement of on-shell boson is enforced by considering only electron-positron pairs with a mass between 70 and 110 GeV/c^2. The PYTHIA Monte Carlo is used to generate events of this process, with the additional requirement that the electrons have a rapidity $|\eta| < 2.7$ and a transverse momentum $p_{\mathrm{T}} > 5$ GeV/c. Of all generated events, 72% are classified as $Z^0\,Z^0$ signal while 26% are ascribed to the $Z^0\gamma^*$ process and 2% to the $\gamma^*\gamma^*$ process.

Taking into account the branching fraction into leptons, $\mathcal{B}$, and the kinematic requirements, ϵ_{KIN}, the relevant NLO cross sections using the MCFM [56] Monte Carlo are:

$$\begin{aligned}
\sigma_{NLO} \times \mathcal{B} \times \epsilon_{KIN}(pp \to W^+Z^0 \to \ell^+\ell^+\ell^-) &= 1034 \text{ fb} \\
\sigma_{NLO} \times \mathcal{B} \times \epsilon_{KIN}(pp \to W^-Z^0 \to \ell^-\ell^+\ell^-) &= 630 \text{ fb} \\
\sigma_{NLO} \times \mathcal{B} \times \epsilon_{KIN}(pp \to Z^0Z^0 \to e^+e^-e^+e^-) &= 18.7 \text{ fb}
\end{aligned}$$

The NLO corrections correspond to k-factors of 1.9 and 1.4 for $W^{\pm}\,Z^0$ and $Z^0\,Z^0$ production, respectively. The NNLO box-diagram contribution to $Z^0\,Z^0$ production is not taken into account.

Three-lepton final-states from $W^{\pm}\,Z^0$ and $Z^0\,Z^0$ production are collected with high efficiency by the Level-1 and HLT electron and muon triggers. The Level-1 and HLT efficiencies for events retained by the selections discussed below is 100% [75].

9.4.3 Background processes

The background to the selection of $W^{\pm}\,Z^0$ and $Z^0\,Z^0$ events comprises other processes with multiple leptons in the final states, some of which might be due to fake signals. The most copious sources of multiple leptons at the LHC are $t\bar{t}$ and $Z^0\,b\bar{b}$ production. The cross section of these processes is large: 830 pb and 1492 pb, respectively, as calculated with MCFM at NLO. These processes may have two leptons in the final states from leptonic decays of the W bosons arising from $t \to Wb$ decays or of the Z^0 boson, respectively. The other leptons can be produced in the direct or cascade decays of the b quarks. The $Z^0\,b\bar{b}$ process is modelled with the COMPHEP Monte Carlo generator [43, 354] and the $t\bar{t}$ process with the TOPREX Monte Carlo program [44]. In addition, the special case in which four electrons are produced in $t\bar{t}$ events is considered in detail and modelled with PYTHIA. Contributions from Wt and $Zc\bar{c}$ to the selected samples are negligible.

Events from $Z^0\,Z^0$ production also constitute a background to the $W^{\pm}\,Z^0$ selection. Events from the $Z^0\gamma^*$ and $\gamma^*\gamma^*$ processes are a background for both the $W^{\pm}\,Z^0$ and $Z^0\,Z^0$ analyses.

9.4.4 $W^{\pm}\,Z^0$ selection

Events with three charged leptons, either electrons or muons, with $p_{\mathrm{T}} > 10\,\mathrm{GeV/c}$ and $|\eta| < 2.5$, are considered by the $W^{\pm}\,Z^0$ selection. All possible Z^0-boson candidates from same-flavours opposite-charge lepton pairs are formed. Events are retained if the mass of the Z^0 candidate is within $20\,\mathrm{GeV/c^2}$ of the Z^0-boson mass, m_Z. These criteria effectively suppress Z^0 decays into tau leptons. The background from $Z^0\,Z^0$ final states is reduced by rejecting events with a second Z^0 candidate with a mass within $40\,\mathrm{GeV/c^2}$ of m_Z. The remaining lepton is associated to the $W^{\pm}$-boson decay; its transverse momentum must be larger than 20 GeV. This criterion results in lower efficiencies for the $W^{\pm}$ boson decays in tau leptons. The highest-p_{T} lepton associated to the Z^0 boson must satisfy $p_{\mathrm{T}} > 15\,\mathrm{GeV/c}$. If the event contains more than three leptons, the lepton with highest p_{T} is chosen as originating from the $W^{\pm}$. The signal efficiency after these cuts is 9.2% while the $t\bar{t}$, $e^+e^-b\bar{b}$ and $\mu^+\mu^-b\bar{b}$ efficiencies are 0.7%, 0.4% and 0.6%, respectively.

Leptons from the decay of b quarks in the background processes are produced in a higher-multiplicity environment and isolation criteria suppress the background contamination. Electrons associated to the $W^{\pm}$ boson must have no other charged track with $p_{\mathrm{T}} > 2\,\mathrm{GeV/c}$ within a $\Delta R = 0.3$ cone around their direction. All muon candidates must have an energy measured in the calorimeters within a $\Delta R = 0.3$ cone around their direction smaller than 5 GeV and the sum of the p_{T} of tracks within a $\Delta R = 0.25$ cone smaller than 2 GeV/c. The significance of the lepton impact parameter in the plane transverse to the beam, S_{IP}, discriminates against leptons from heavy-quark decays. This variable is defined as the ratio between the measured impact parameter and its uncertainty and is required to satisfy $S_{IP} < 3$. The signal efficiency after these cuts is 7.3% while the $t\bar{t}$, $e^+e^-b\bar{b}$ and $\mu^+\mu^-b\bar{b}$ efficiencies are 0.07%, 0.008% and 0.03%, respectively.

The $t\bar{t}$ and $Z^0\,b\bar{b}$ final states are associated with one or more hard jets and their contribution is reduced by removing events containing at least a jet with $E_{\mathrm{T}} > 25\,\mathrm{GeV}$. Only jets outside cones of $\Delta R = 0.3$ around the three leptons are considered. The reconstructed mass of the Z^0 boson is required to be within $10\,\mathrm{GeV/c^2}$ of m_Z, leading to the total efficiencies presented in Table 9.8.

9.4.5 $Z^0\,Z^0$ selection

The $Z^0\,Z^0$ selection is based on events with four electrons, identified from superclusters in the electromagnetic calorimeter matched with a charged track. The transverse momenta of the electron candidates, ordered from the largest to the smallest, have to be above 30 GeV/c, 20 GeV/c, 15 GeV/c and 10 GeV/c, respectively. This cut suppresses the contribution from the $Z^0\gamma^*$ and $\gamma^*\gamma^*$ final states and reduces by 30% and 60% the $t\bar{t}$ and $Z^0\,b\bar{b}$ backgrounds, respectively. Leptons from b quarks decays in the $t\bar{t}$ and $Z^0\,b\bar{b}$ background processes are produced in association with hadrons. Their contribution is reduced by requiring the electrons to be isolated: the ratio between the energy deposited in the hadronic and the electromagnetic calorimeters must be below 8%; no more than two other charged track with $p_{\mathrm{T}} > 2\,\mathrm{GeV/c}$ must be within a $\Delta R = 0.3$ cone around the electron; $\Sigma_i(p^i_{\mathrm{T}} - E_{\mathrm{T}})_i/E_{\mathrm{T}} < 0.34$, where E_{T} is the transverse energy of the electron candidate and the sum runs on all tracks with $p_{\mathrm{T}} > 2\,\mathrm{GeV/c}$ within a $\Delta R = 0.3$ cone around the electron.

Electron-positron pairs are combined to form Z^0 candidates. Pairs with reconstructed masses between 50 and $120\,\mathrm{GeV/c^2}$ are retained. Of the two possible $Z^0\,Z^0$ pairings, the one where the Z^0 candidate masses are closest to m_Z is chosen. This pairing is correct for almost all

events with two on-shell Z^0 bosons. For 2.5% of the events, more than four electrons are present and only the Z^0 Z^0 pairing which contains the highest-p_{T} electron is retained. Table 9.9 presents the signal and background selection efficiencies.

Table 9.8: Yield of the $W^{\pm}$ Z^0 selection for an integrated luminosity of $1\mathrm{fb}^{-1}$. Signal efficiencies include gauge-boson decays into tau leptons.

	$e^{\pm}e^{+}e^{-}$	$\mu^{\pm}e^{+}e^{-}$	$e^{\pm}\mu^{+}\mu^{-}$	$\mu^{\pm}\mu^{+}\mu^{-}$	Total	Efficiency
$W^{\pm}Z^0 \to \ell^{\pm}\ell^{+}\ell^{-}$	14.8	26.9	28.1	27.0	96.8	6.1%
Z^0Z^0	0.63	1.54	1.50	1.51	5.18	4.7%
$t\bar{t}$	0.93	1.55	–	0.31	2.79	0.02%
$\mu^{+}\mu^{-}b\bar{b}$	–	–	6.54	4.9	11.4	0.005%
$e^{+}e^{-}b\bar{b}$	1.21	1.82	–	–	3.03	0.005%

Table 9.9: Yield of the Z^0 Z^0 selection for integrated luminosities of $1\,\mathrm{fb}^{-1}$ and $10\,\mathrm{fb}^{-1}$. The last row indicates the signal significance, which include systematic effects.

	Efficiency	$N_{\mathrm{events}}/1\,\mathrm{fb}^{-1}$	$N_{\mathrm{events}}/10\,\mathrm{fb}^{-1}$
Z^0 Z^0	38%	7.1	71.1
$Z^0\gamma^*$	4.5%	0.16	1.60
$Z^0b\bar{b}$	0.07%	0.08	0.84
$t\bar{t}$	0.06%	0.12	1.22
S_L		4.8	13.1

9.4.6 Systematic uncertainties

For the first $1\,\mathrm{fb}^{-1}$ of integrated luminosity, the total systematic uncertainties on the $W^{\pm}$ Z^0 and Z^0 Z^0 cross section measurements are 17.4% and 12.9%, respectively. These figures include a 10% uncertainties on the determination of the integrated luminosity.

The most important sources of systematic uncertainties are lepton identification and isolation, and background subtraction. A 2% uncertainty on the efficiency of each lepton propagates to an uncertainty on the cross section between 2.6% and 7.8%, according to the channel. Background subtraction dominates the $W^{\pm}$ Z^0 systematics with an uncertainty of 12%, while it accounts for a 1.3% uncertainty in the Z^0 Z^0 channel. An additional uncertainties of 5% on the jet energy scale affects the $W^{\pm}$ Z^0 channel, while an uncertainty of 1% on the trigger efficiency affects both channels.

The significance of the observation of the $W^{\pm}$ Z^0 and Z^0 Z^0 signals in the first $1\,\mathrm{fb}^{-1}$ is not sensitive to the luminosity uncertainty. It is affected by all other sources of systematic uncertainty listed above, with a total effect of 14.8% and 14.2% on the two channels, respectively. These uncertainties include additional PDF and QCD uncertainties in the Monte Carlo modelling, contributing 3.7% and 6.4% for the $W^{\pm}$ Z^0 and Z^0 Z^0 selections, respectively.

9.4.7 Results

Figure 9.11 left presents the mass distribution of the Z^0 candidates in the $W^{\pm}$ Z^0 channel for an integrated luminosity of $1\,\mathrm{fb}^{-1}$ before the last requirement of a $\pm 10\,\mathrm{GeV/c}^2$ window is applied. A large signal-over-background ratio is observed, as shown in Table 9.8.

Figure 9.11 right shows the mass distribution of the Z^0 candidates, two entries per event, selected by the $Z^0\ Z^0$ selection for an integrated luminosity of $10\,\text{fb}^{-1}$. Table 9.9 lists the selection yield for $1\,\text{fb}^{-1}$ and $10\,\text{fb}^{-1}$. The selection results into an almost background-free signal sample, which will constitute a valuable input to assess the background in the search for the Higgs boson.

Both the $W^{\pm}\ Z^0$ and $Z^0\ Z^0$ final states can be selected with high purity. A significance of 12.8 and 4.8, respectively, is expected in the first 1fb^{-1} of integrated luminosity, including systematic uncertainties. The $W^{\pm}\ Z^0$ channel can be observed with a significance of 5, including systematic effects, in an integrated luminosity of $150\,\text{pb}^{-1}$.

This study of multiple gauge-boson production and couplings at the LHC will be extended to include the $W^{\pm}\gamma$ and $Z^0\gamma$ channels, as well as the other flavours of $Z^0\ Z^0$ fully-leptonic decays.

In conclusion, the large signal-over-background ratios achieved by the $W^{\pm}\ Z^0$ and $Z^0\ Z^0$ selections suggest that early observation of these channels will take place at the LHC start up. In addition, precise investigations of triple gauge-boson couplings will be possible with the first $10\,\text{fb}^{-1}$ of LHC data.

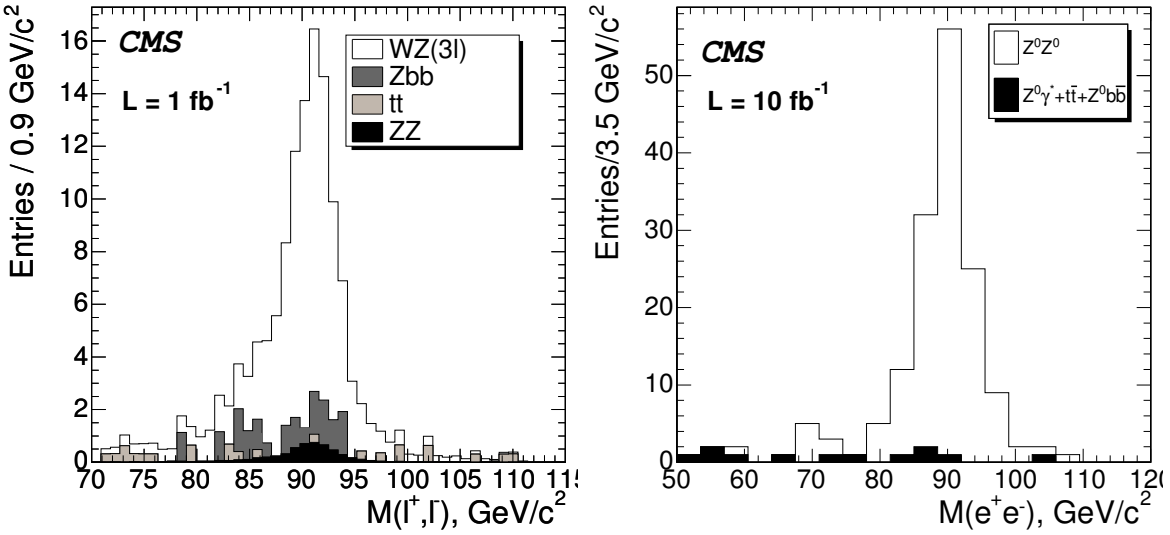

Figure 9.11: Left: Distribution of the mass of the Z^0 candidates for events retained by the $W^{\pm}\ Z^0$ selection, for an integrated luminosity of $1\,\text{fb}^{-1}$. Right: Distribution of the mass of the Z^0 candidates, two entries per event, retained by the $Z^0\ Z^0$ selection, for an integrated luminosity of $10\,\text{fb}^{-1}$.